Journal of Energy Storage 14 (2017) 168–178

Contents lists available at ScienceDirect

Journal of Energy Storage

journal homepage: www.elsevier.com/locate/est

System theoretic analysis of battery charging optimization

Tyrone L. Vincent[a,*], Peter J. Weddle[b], Gongguo Tang[a]

[a] Department of Electrical Engineering, Colorado School of Mines, Golden, CO 80401, United States
[b] Department of Mechanical Engineering, Colorado School of Mines, Golden, CO 80401, United States

ARTICLE INFO

Article history:
Received 26 June 2017
Received in revised form 4 September 2017
Accepted 6 September 2017
Available online 20 November 2017

Keywords:
Lithium-ion batteries
Systems modeling and analysis
Optimal charging

ABSTRACT

Innovative optimal charging sequences are sought to minimize battery degradation and reduce charging loses. One charging sequence under investigation incorporates high frequency pulses or sinusoidal perturbations. However, there is disagreement in the literature on the benefits/disadvantages of pulsed charging. This work analytically determines optimal battery charging sequences for two cases: minimizing energy losses and maximizing charge supplied to the battery while respecting lithium plating constraints. Assuming relevant battery physics have linear, time-invariant dynamic behavior, optimal charging strategies are derived analytically. The analysis exposes specific features of the battery dynamic response (frequency response and impulse response) that must be present for optimal charging sequences to have periodic components. In the case of energy minimization, the battery's electrochemical impedance must approach the imaginary axis. In the case of limiting lithium plating, a criterion is developed involving impulse responses of relevant battery variables.

1. Introduction

Lithium-ion batteries have attractive features for many applications, and are widely used as high energy density storage devices. The internal electrochemical and chemical reactions occurring during charge/discharge make Li-ion batteries sensitive to demand sequences and operating conditions [1]. Because cells are sensitive to system demands and operating conditions, battery management systems are developed to keep cells within acceptable operating ranges to prolong life, reduce charging losses, and mitigate failure [2,3]. This paper uses analytical tools to provide analysis and insight into optimal charging profiles proposed by the research community to better inform battery management systems.

A particular area of interest in the research community are charge/discharge protocols that incorporate pulses or sinusoidal perturbations. Experimental and simulation evidence has been published arguing that pulsed charging optimally charges/discharges cells [4–9], while others have argued that pulsed charging has no effect or hinders performance [10–12]. It can be argued that experimental results evaluating pulsed charging are subtle enough that experimental conditions and uncertainty can result in both positive and negative interpretation. A physical, mechanistic explanation for the positive effects of perturbations is a key element to guiding further work.

There are several ways to evaluate 'optimal' charging. This paper will focus on two particular criteria for optimal charging: efficiency of charging and reduction of lithium plating. The goal of this paper is to use basic system theoretic analysis to determine optimal charging sequences and evaluate mechanisms that contribute to the 'shape' of optimal pulsed charging sequences.

1.1. Increasing charging efficiency

It has been argued that sinusoidal/pulse sequences increase the charging efficiency, meaning less energy is required to charge a battery to a desired state-of-charge. Some explanations provided in the literature include:

- If a sinusoidal perturbation is chosen at the frequency where the electrochemical impedance is minimized, " . . . the energy loss in electrical energy transfer to chemical energy is minimized" [7].
- If a sinusoidal perturbation is chosen in the correct frequency range, " . . . concentration polarization in the electrodes is minimized because charge accumulation is reduced" [9]. That is, a phase shift occurs between peak current and peak concentration polarization.
- Pulsed charging with a rest period allows "ions to diffuse and distribute electrolyte ions more evenly to change the

* Corresponding author.
E-mail addresses: tvincent@mines.edu (T.L. Vincent), pweddle@mines.edu (P.J. Weddle), gtang@mines.edu (G. Tang).

http://dx.doi.org/10.1016/j.est.2017.09.009
2352-152X/

concentration at the surface of the electrode" increasing the exchange current density [5].

1.2. Reduction of lithium plating

Sinusoidal/pulse sequences are also argued to minimize aging due to lithium plating. Two (related) explanations for this are:

- Pulsing reduces lithium concentration at the electrode interface. "The proposed pulse sequence enables higher charging rates, without ever reaching lithium saturation" [4].
- Pulsing reduces the polarization voltage. "Large polarization not only renders the battery undercharged but also results in active material loss" [8].

1.3. Scope of this paper

This paper provides an answer to the following question: What are the features of a battery, as a linear dynamic system, that must be present for optimal charging strategies to include oscillatory components such as pulses or sinusoids? The results will, in fact, provide evidence against several of these mechanistic explanations given above regarding the benefits of pulsed charging. Of course, the restriction to linear dynamics limits the scope of our conclusions. However, within this limited scope, we believe this analysis provides useful insight into how battery dynamic behavior impacts optimal charging sequences, and can provide a starting point for interpreting the results of experimental and numerical results of higher fidelity.

1.4. Related work

A standard charging protocol for Li-ion batteries is to charge the battery at a constant current until a voltage limit is reached. Once the voltage limit is reached, the current is reduced to maintain this maximum voltage. This protocol is called constant-current/constant-voltage (CC–CV) charging [13]. While simple to implement and widely used, it is primarily derived from basic principles of battery operation. There are efforts seeking to optimize these charging sequences to reduce charging time, increase charging efficiency, and other objectives. The most systematic analysis involves numerically searching for an optimal charging sequence using a battery model [14–21]. These methods investigate optimization of a variety of cost functions, including charging time and charging energy. Constraints include internal temperature, terminal voltage, and overpotential. Since these methods do not result in an optimal charging sequences that contain an oscillatory component, it can call into question whether pulsed or sinusoidal charging is truly useful. On the other hand, these numerical methods only provide the optimal sequence for a specific battery model, limiting their ability to provide general insight. In addition, it can also be argued that an optimal charging current containing a periodic component can be lost in numerical error, especially if the periodic component is relatively high frequency.

The current paper provides a different type of analysis, that while not capturing all possible battery behavior, does address *dynamic* effects that are captured by linear models. This paper does not purport to offer an alternative method for numerically finding an optimal charging sequence, but instead uses analytic results to provide insight between battery dynamics and the qualitative behavior of the optimal charging sequence.

1.5. Notation

$j \equiv \sqrt{-1}$. L_2 is the set of square integrable functions. L_1 is the set of absolutely integrable functions. $L_2[0, T]$ is the set of functions square integrable over the domain $[0, T]$. For a complex number x, $\mathrm{Re}\{x\}$ is the real part and $\mathrm{Im}\{x\}$ is the imaginary part. For a function $x(t)$, $\mathcal{L}\{x(t)\}$ is the one-sided Laplace Transform of $x(t)$,

$$\mathcal{L}\{x(t)\} = \int_0^\infty x(t)e^{-st}dt. \tag{1}$$

$\mathcal{L}^{-1}$ is the inverse Laplace transform operator.

2. Analysis of energy optimal charging

To evaluate charging sequences that minimize losses, consider a battery model consisting of a linear circuit element in series with a non-linear capacitive element. The non-linear capacitive element models the open circuit voltage as a function of state of charge, while the linear circuit models transient effects, such as diffusion and charge transfer. To charge the battery, a current $i(t)$ is supplied, which in turn causes a response in the terminal voltage $v(t)$. Based on the modeling assumptions, the battery's electrical response has the following relationships between applied current, voltage, and state of charge

$$v(t) = \int_0^T g(t-\tau)i(\tau)d\tau + v_{\mathrm{oc}}(s_{\mathrm{c}}(t)), \tag{2}$$

$$s_{\mathrm{c}}(t) = s_{\mathrm{c}}(0) + \frac{1}{Q_0}\int_0^t i(\tau)d\tau, \tag{3}$$

where $g(t)$ is the impulse response of the linear element (that is, the voltage trajectory across the element due to a short pulse of current through the element), T is the total amount of charging time, and v_{oc} is the open circuit voltage, which is a function of the state of charge $s_{\mathrm{c}}(t)$. The integral involving $g(t)$ and $i(t)$ is a convolution, and is a time-domain solution for the response of a linear system with impulse response $g(t)$ to the input signal $i(t)$ [22]. The state of charge, in turn, is the integral of the applied current, normalized by the charge at full capacity, Q_0, plus the initial state of charge $s_{\mathrm{c}}(0)$.

There are many different physical behaviors that contribute to battery dynamics, including diffusion of lithium and lithium ions in anode and cathode, charge transfer across double layers that develop at electrode/electrolyte interfaces, and electrochemical reactions associated with lithium intercalation, among others. In this model, the internal processes (i.e., polarization and chemical kinetics) are exposed only through their influence on the terminal voltage. However, when trying to minimize charging losses (i.e. maximize charging *efficiency*) the terminal voltage completely specifies the energy required to supply a given current, and thus reflects all internal losses or chemical efficiency inside a cell. In the literature, battery models that predict the terminal voltage are often modeled using lumped equivalent circuit models. Fig. 1 shows a relatively simple equivalent circuit model interpreted from the literature [12], with parameters shown in Table 1. In this case, the open circuit voltage is modeled by a voltage V_0 representing the voltage at low state of charge, and a capacitor providing a linear increase in open circuit voltage with respect to state of charge. While this simple equivalent circuit model will be used as an example, our results apply to any general open circuit voltage relationship.

As will be shown, the existence or non-existence of an optimal charging sequence containing a sinusoidal component is determined by the battery's frequency response. For batteries, the

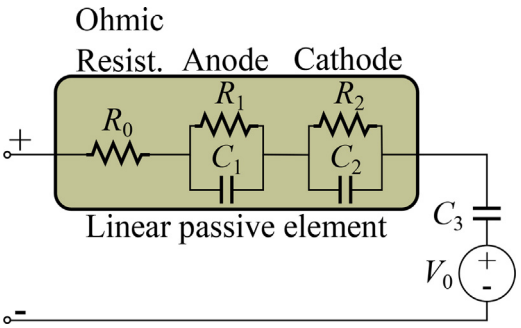

Fig. 1. Example of a Li-ion battery equivalent circuit model.

Table 1
Parameters for the Li-ion battery equivalent circuit model.

Linear element	Variable	Value [12]
Ohmic resist.	R_0 [Ω]	0.105
Anodic resist.	R_1 [Ω]	0.028
Cathodic resist.	R_2 [Ω]	0.018
Anodic cap.	C_1 [F]	0.1
Cathodic cap.	C_2 [F]	2
OCV cap.	C_3 [F]	1

frequency response is an important diagnostic found by impedance spectroscopy [11]. As is well known, a linear element with impulse response $g(t)$ (see (2)) has a frequency response/impedance spectrum of $G(j\omega)$ where $G(s) = \mathcal{L}\{g(t)\}$ [22].

The frequency response is found experimentally using a process called electrochemical impedance spectroscopy. The frequency response, or impedance, is plotted as a polar plot with axes $\mathrm{Re}\{G(j\omega)\}$ and $-\mathrm{Im}\{G(j\omega)\}$ [11]. Fig. 2 illustrates the impedance for the battery equivalent circuit model of Fig. 1 with parameters from Table 1. The plot shows both the spectral impedance of the battery, which includes the open circuit voltage response ($\tilde{G}(j\omega) = G(j\omega) + 1/(j\omega C_3)$), and the spectral impedance of the linear circuit alone ($G(j\omega)$). Note that the linear circuit elements do not include the storage component of the battery response, and the impedance of $G(j\omega)$ at relatively low frequencies has no capacitance, while the impedances become equal at high frequency.

A property that can be observed in Fig. 2, and is characteristic of the impedance spectra for all realistic batteries, is that the polar plot does not cross the imaginary axis. This property is captured in the following definition.

Definition 1. The complex function $G(j\omega)$ is *strictly positive real* if there exists ε such that $\mathrm{Re}\{G(j\omega)\} > \varepsilon$ for all ω.

2.1. Assumptions

In what follows, the following are assumed:

- The impulse response of the linear circuit element is $g(t)$.
- The linear circuit element is bounded-input, bounded-output stable, or equivalently, $g(t)$ is absolutely integrable: $\int_0^\infty |g(t)|dt < \infty$.
- $G(s) = \mathcal{L}\{g(t)\}$ with $G(j\omega)$ strictly positive real.

2.2. Minimizing charging losses

A charging sequence is sought that minimizes the energy required to supply a net charge of Q to the battery over fixed time interval T. The energy required to charge the battery is given by the integral of the product of the terminal voltage and current. This

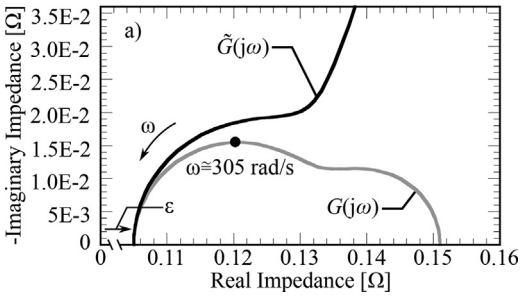

Fig. 2. Impedance spectra $\tilde{G}(j\omega)$ and the impedance spectra with the battery storage removed, $G(j\omega)$. Model structure and parameters are given in Fig. 1 and Table 1.

optimization problem can be expressed as

$$\begin{aligned} \min_{i(t)\in L_2[0,T]} \quad & \int_0^T i(t)v(t)dt, \\ \text{subject to} \quad & \int_0^T i(t)dt = Q, \ (2) \text{ and } (3), \end{aligned} \tag{4}$$

where $L_2[0, T]$ is the set of all square-integrable functions with support on the interval $[0, T]$.

In the following theorems the minimizer of (4) and the frequency response of the linear circuit element are related. First, Theorem 1 gives an integral equation that the optimal solution must satisfy. Then, based on the similarity between this integral equation and the Wiener–Hopf equation, Theorem 2 gives a method for finding the solution directly from the Laplace transform of the impulse response.

Theorem 1. *Given $\xi(t)$ the solution to*

$$\int_0^T \xi(t)(g(t-\tau) + g(\tau - t))dt = 1, \tag{5}$$

for all $\tau \in [0, T]$. The minimizer of (4) is $i(t) = (Q/\beta)\xi(t)$ where $\beta = \int_0^T \xi(t)dt$.

Proof. See Appendix □

Eq. (5) defines the optimal charging sequence as the solution to an integral equation. It turns out that this equation is similar to a well studied equation in systems theory: the Weiner–Hopf equation, which has the form

$$\int_0^\infty h(t)(g(t-\tau) + g(\tau - t))dt = 1. \tag{6}$$

Note that when $T = \infty$, the equations are the same. The solution $h(t)$ to (6) can be found using the Weiner–Hopf method, which utilizes $G(s)$, and thus is a frequency domain representation of the solution. This method, in the case when $G(s)$ can be represented as a rational function,[1] is as follows [23]:

- Write $G(s)$ as $G(s) = N(s)/D(s)$, where $N(s)$ and $D(s)$ are polynomials.
- Write $G(s) + G(-s)$ with common denominator as $R(s)/(D(s)D(-s))$ where $R(s) = N(s)D(-s) + N(-s)D(s)$.
- Factor $R(s)$ as $R(s) = R_+(s)R_-(s)$ where the roots of $R_-(s)$ are in the left half plane, and the roots of $R_+(s)$ are in the right half plane.[2]
- The solution is

$$h(t) = \left(\frac{D(0)}{R_+(0)}\right)\mathcal{L}^{-1}\left\{\frac{D(s)}{R_-(s)s}\right\}. \tag{7}$$

[1] A rational function is a ratio of polynominals.
[2] If $R(s)$ has roots on the $j\omega$ axis, they are repeated, and can be distributed equally between $R_-(s)$ and $R_+(s)$).

This formulation is useful because it provides insight on the form of the optimal solution. In particular, let $p_i, i = 1, \ldots, n$, be the roots of $R_{-}(s)$. Then

$$h(t) = A_0 + A_1 e^{p_1 t} + A_2 e^{p_2 t} + \cdots + A_n e^{p_n t} \tag{8}$$

where A_i are constants. When the roots p_i are complex, they will bein complex conjugate pairs, and this pair can be combined into a single term of the form $Be^{\sigma t}\cos(\omega \bar{t} + \theta)$, where $\sigma = \mathrm{Re}\{p_i\}$. Thus, *for the optimal current to have a sinusoidal term with magnitude that decays no faster than a time constant of (say) t_0 seconds, the roots of $R(s)$ must have a (negative) real part with magnitude less than $1/t_0$.*

With finite T, the Weiner–Hopf solution can also be used to obtain an approximate solution, with approximation error that decreases with increasing T, as long as $g(t)$ satisfies an additional condition that is typically always satisfied for battery spectra.

Theorem 2. *If for any finite ω, $\mathrm{Re}\{G(j\omega)\} \geq \lim_{\omega\to\infty} G(j\omega)$, the solution to (5) is*

$$\xi(t) = \zeta(t) + w_T(t), \tag{9}$$

where

$$\zeta(t) = \begin{cases} h(t) & 0 \leq t \leq \dfrac{T}{2} \\ h(T-t) & \dfrac{T}{2} < t \leq T \end{cases}, \tag{10}$$

and

$$\lim_{T\to\infty} \frac{1}{T} \int_0^T w_T^2(t)dt = 0. \tag{11}$$

Proof. See Appendix □

Theorems 1 and 2 indicate that an optimal charging sequence of length T will have a significant sinusoidal component if and only if $R(s) = 0$ for some s with the magnitude of the real part on the order of $1/T$. Since $R(s)/(D(s)D(-s)) = G(s) + G(-s)$, the finite values of s for which $R(s) = 0$ are the same as for which $G(s) + G(-s) = 0$. Since $G(s)$ represents a stable system, $G(s)$ is an analytic function near the $j\omega$ axis, and can be represented via a Taylor Series expansion around $j\omega$ that uses only information from $G(j\omega)$ [24], namely

$$G(\sigma + j\omega) = G(j\omega) + \sum_{k=1}^{\infty} \frac{1}{k!} \frac{d^k G(j\omega)}{j^k d\omega^k} \sigma^k. \tag{12}$$

Let $F(s) = G(s) + G(-s)$. Then

$$F(\sigma + j\omega) = 2\mathrm{Re}\{G(j\omega)\} + \sum_{k=1}^{\infty} \frac{2(-1)^k}{2k!} \frac{d^{2k}\mathrm{Re}\{G(j\omega)\}}{d\omega^{2k}} \sigma^{2k} + \sum_{k=0}^{\infty} \frac{-2j(-1)^k}{(2k+1)!} \frac{d^{2k+1}\mathrm{Re}\{G(j\omega)\}}{d\omega^{2k+1}} \sigma^{2k+1}.$$

Significant sinusoidal components appear in the optimal current when $F(\sigma + j\omega) = 0$. Since both the real and imaginary part must be zero, a necessary condition based on the real part is

$$\mathrm{Re}\{G(j\omega)\} = -\sum_{k=1}^{\infty} \frac{(-1)^k}{2k!} \frac{d^{2k}\mathrm{Re}\{G(j\omega)\}}{d\omega^{2k}} \sigma^{2k}. \tag{13}$$

When $G(j\omega)$ is smooth, it can be well represented using just a few terms from the Taylor Series. Under the assumption that four terms are sufficient (implying accuracy up to order σ^5), (13) can be rearranged to give the following closed form equation for σ:

$$\sigma = -\sqrt{\frac{2\mathrm{Re}\{G(j\omega)\}}{\frac{d^2\mathrm{Re}\{G(j\omega)\}}{d\omega^2}}}. \tag{14}$$

In other words, if $R(s)$ has a root near $j\omega$, then the real part must be as given by (14). Thus, *unless the ratio of $2\mathrm{Re}\{G(j\omega)\}$ to $\frac{d^2\mathrm{Re}\{G(j\omega)\}}{d\omega^2}$ is positive and on the order of $1/T^2$, the optimal charging sequence will not have a significant sinusoidal component.*

2.3. Illustrative optimal charging sequence

The results of the previous section are illustrated for the equivalent circuit model (see Fig. 1) with parameters from Table 1. The key outcome of Theorems 1 and 2 is that the character of the optimal charging sequence can be predicted from the impedance frequency response. Fig. 3 shows $2\mathrm{Re}\{G(j\omega)\}$ and $\frac{d^2\mathrm{Re}\{G(j\omega)\}}{d\omega^2}$ plotted vs ω, along with σ calculated by (14) at each frequency. Note that $\frac{d^2\mathrm{Re}\{G(j\omega)\}}{d\omega^2}$ is negative for frequencies less than 10 rad/s; in this frequency range there are no complex roots of $F(s)$. When $\frac{d^2\mathrm{Re}\{G(j\omega)\}}{d\omega^2}$ is positive, it is quite small, less than 2×10^{-5}. This results in σ being large with the minimum value greater than 100 (see Fig. 3c). This means that any oscillatory term of $h(t)$ will decay with a time constant smaller than 10 ms.

The optimal current trajectory is found by solving (5) and/or (10). Fig. 4 illustrates the exact optimal charging sequence (given by (5)) and the approximate solution (given by (7) and (10)) for $Q = 1$ A-s and several values of charging time T. Here the charging time has been chosen to be very small to accentuate the effects of the optimal input. Note that the differences between (5) and (10) are very small, even for this short charging time. The optimal charging sequence is very close to a constant current, except the optimal current is larger at the very beginning and very end of the trajectory.

The optimal charging strategy for $T = 1$ s is applied to the equivalent-circuit battery model at 0% SOC and $V(0) = 3.2$ V. The energy consumed in charging the battery is then monitored for both the optimal charging strategy and constant current case (where the constant current case has an input of $i(t) = Q/T$ for the entire charging time). Fig. 5 illustrates the voltage response and cumulative energy needed to charge the cell (i.e. $\int_0^t i(\tau)v(\tau)d\tau$) at

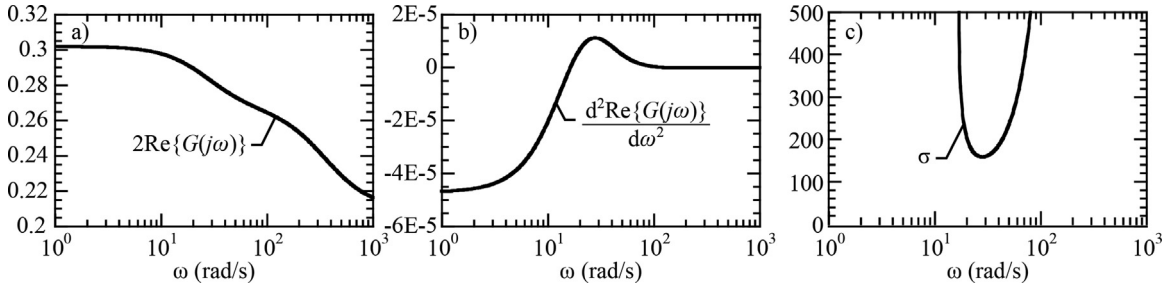

Fig. 3. System responses for the equivalent circuit model. (a) Illustrates twice the real part of the frequency impulse response. (b) Illustrates the second derivative of the real part of the frequency impulse response with respect to frequency. (c) Illustrates the sinusoidal damping coefficient with respect to frequency (see (14)).

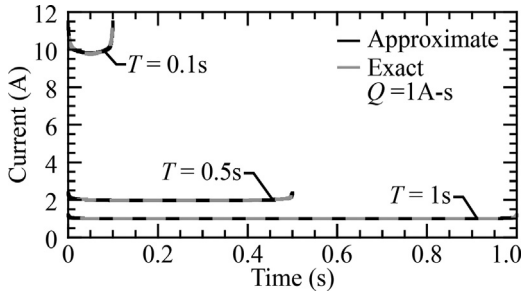

Fig. 4. Optimal charging current strategy to minimize energy loss. Both the exact and approximate solutions are presented for charging times of 0.1, 0.5, and 1 s. In all cases, the cell is charged 1 C.

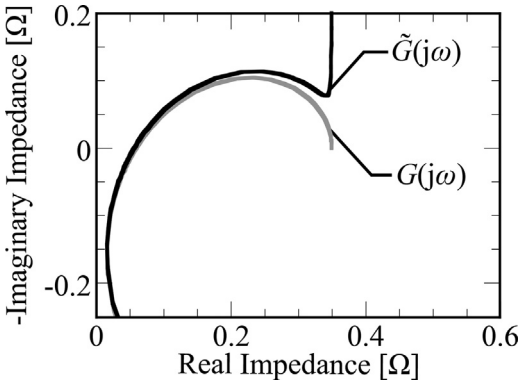

Fig. 6. Non-typical battery impedance spectra that will produce an optimal charging strategy with sinusoidal behavior.

the very beginning and very end of the charging time. Because the optimal current is initially larger, it induces a higher voltage and requires more energy at the beginning of the charging sequence. However, this is offset by a (slightly) reduced current for the majority of the charging time, and the cumulative energy is reduced at the end of the charging sequence, although the reduction is very modest. Note that voltage constraints were not considered in this problem - only efficiency. If a constraint on the maximum applied voltage were added, the current would initially be similar to the optimal current, but would then decrease in the same manner as the constant voltage portion of the CC–CV charging protocol.

For a more realistic charging time, the results would be similar. The most important take-away from the point of view of this paper is that the optimal charging sequences did *not* include a sinusoidal or other periodic component. The results of this paper argue that optimal sinusoidal current trajectories can be predicted *merely from observing that the impedance spectra of batteries do not approach the imaginary axis.*

2.4. Example of impedance spectra that predicts sinusoidal optimal charging

To illustrate how an impedance that does approach the imaginary axis can give rise to oscillatory components, consider the impedance shown in Fig. 6, which is the polar plot of the impedance for $G(s) = \left((s+\sqrt{10})^2 + 1000\right)/(s+17\sqrt{10})^2$. This impedance is not typical of batteries, because the ohmic resistance is usually active at all frequencies, preventing the impedance from approaching the imaginary axis. Fig. 7 shows $2\mathrm{Re}\{G(j\omega)\}$ and $\frac{d^2\mathrm{Re}\{G(j\omega)\}}{d\omega^2}$ plotted vs ω, along with σ calculated by (14) at each frequency. In this case, because $\mathrm{Re}\{G(j\omega)\}$ becomes very small, σ has a minimum of about 7 at 40 rad/s. In fact, because the exact form of $G(s)$ is available, $R(s)$ can be calculated exactly, and has double root at $s = -7 \pm 40.7j$. Thus, the optimal current does contain a (damped) sinusoidal component that decays with a time constant of 1/7 s. The optimal current trajectory as predicted by (5) and approximated by (10) is illustrated in Fig. 8. For the sinusoidal term to decay more slowly, the system impedance would need to come even closer to the imaginary axis.

2.5. Discussion

When battery dynamics are well approximated by a linear model, the charging sequence that requires minimum energy to insert a given amount of charge will not have a periodic component unless (14) is very small for some frequency. Since the impedance spectra for all real batteries contains a contact resistance element that keeps the real part of the impedance from approaching zero, it is unlikely a periodic current will be optimal in reducing losses. Thus, any explanation for the benefit of sinusoidal or other periodic sequences imposed on charging trajectories is not valid if the physics are captured by linear elements. Since both concentration

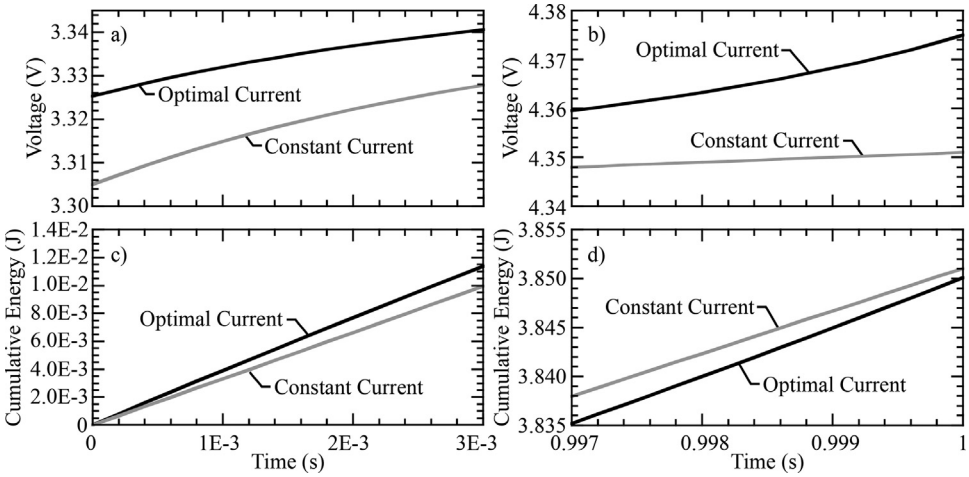

Fig. 5. Voltage response and cumulative energy expended during optimal current and constant current charging strategies ($Q = 1$ A-s and $T = 1$ s). (a and b) Illustrate the voltage responses at the beginning and end of charging respectively. (c and d) Illustrate the cumulative energy consumed at the beginning and end of charging respectively.

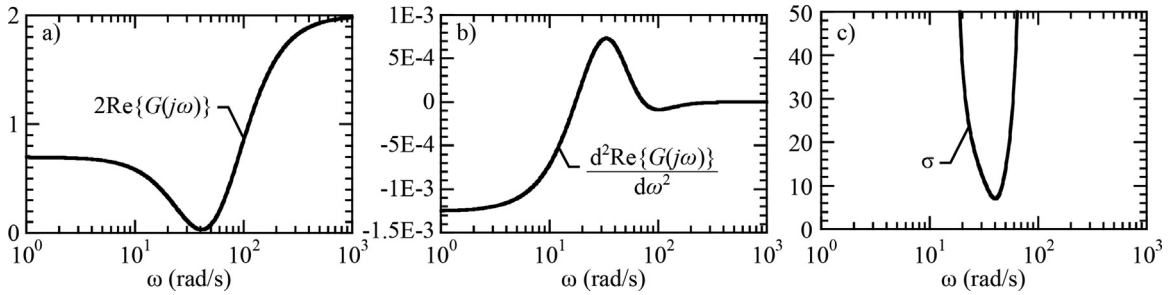

Fig. 7. System responses for the example model. (a) Illustrates twice the real part of the frequency impulse response. (b) Illustrates the second derivative of the real part of the frequency impulse response with respect to frequency. (c) Illustrates the sinusoidal damping coefficient (see (14)).

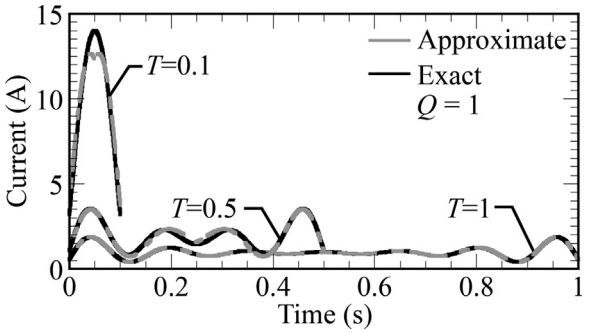

Fig. 8. Exact and approximate optimal current profiles at various charging times $T = 0.1, 0.5, 1$ s and a specified charge supplied $Q = 1$ A-s. This optimum is found using the a non-typical battery equivalent circuit whose impedance response is shown in Fig. 6.

polarization and lithium diffusion can be well modeled using linear elements, these behaviors by themselves will not contribute towards any benefit for pulse charging. More specifically, relative phase shifts between peak current and peak concentration polarization or lithium concentration induced by periodic perturbations will not result in optimal charging, in terms of minimizing losses. Of course, it may still occur that *nonlinear* effects may imply a benefit from pulse charging. For example, one scenario where an oscillatory component is found to be optimal via numerical optimization is when discharging a battery at low temperature [25–27]. In these studies, the sinusoidal charging sequences increased the internal battery temperature, which resulted in a decrease in the battery's internal resistance. This is a strongly nonlinear effect that is not captured by our analysis. Another example of a strongly nonlinear effect is hysteresis of the open circuit potential [28], although to the authors knowledge there has not been an attempt to link this effect to charging efficiency. Finally, we note that battery dynamics modeled well by linear elements at low charging rates may not be modeled well at high charge rates.

3. Analysis of charging while meeting constraints

A second explanation for obtaining a benefit when using charging sequences with periodic components is related to lithium plating and/or overcharging, where it is argued that potentials contributing to plating can be reduced or controlled through pulsing. In what follows, an analysis of this effect is presented.

When charging, the applied current $i(t)$ induces trajectories for internal variables whose magnitudes are related to a propensity for lithium plating. The objective is to charge the battery while maintaining appropriate bounds on these variables. In this study, when the overpotential on the anode surface is equal to or exceeds the open-circuit potential (OCP) of graphite vs lithium metal, it is assumed that the formation of lithium metal is more chemically favorable than lithium intercalation. In this case, the overpotential η is defined as the potential difference between the anode and electrolyte with respect to an equilibrium potential. Fig. 9 illustrates the OCP for a graphite anode with respect to lithium metal [29]. Overlaid on the figure is an imposed linear overpotential limit that approximates the OCP curve. Of course the true condition for lithium plating is a result of chemical kinetics on the anode/electrolyte surface [30,13]. However, this overpotential limit as a function of intercalation fraction is a reasonable first approximation [31,13].

To capture this desired behavior, the constraint.

$$\eta(t) \leq \eta_0 - (\eta_0 - \eta_1)x(t) \tag{15}$$

is proposed, where $x(t)$ is the surface concentration (which varies between 0 and 1), η_0 is the bound at $x = 0$, and η_1 is the bound at $x = 1$.

3.1. Optimal charging with overpotential constraints

To obtain analytical solutions for optimal charging with respect to internal constraints, the battery internal variables are assumed to have linear dynamics. Thus, the overpotential $\eta(t)$ is given by

$$\eta(t) = \int_0^t g_\eta(t-\tau)i(\tau)d\tau, \tag{16}$$

where $g_\eta(t)$ is the impulse response of η to input i. The intercalation fraction of lithium on the surface of the anode $x(t)$ is also a dynamic process because of surface reactions and diffusion into the anode particles. In a general linear model the intercalation fraction can be expressed as

$$x(t) = \int_0^t g_x(t-\tau)i(\tau)d\tau + x(0), \tag{17}$$

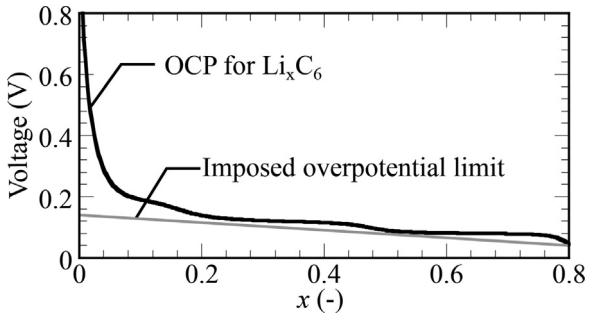

Fig. 9. Anode open circuit potential vs. lithium metal as a function of intercalation fraction [29]. Overlaid is a proposed voltage limit to avoid plating on the anode surface.

where $g_x(t)$ is the impulse response of x to input i, and $x(0)$ is the surface intercalation fraction at the start of charging.

Using these assumptions, consider an optimal charging sequence over fixed time T. In this case, optimal means that the charging sequence will maximize the amount of charge delivered in time T, while meeting the constraint on overpotential (see (15)). This optimization can be expressed as

$$\begin{aligned} \max_{i(t)\in L_2[0,T]} \quad & \int_0^T f(T-t)i(t)dt, \\ \text{subject to} \quad & \eta(t) \le Af(t) - B\,\mathrm{x}(t), \\ & (16), \text{ and } (17). \end{aligned} \tag{18}$$

Note that the function $f(t)$ has been introduced as a weighting on the integral of the current and the constraint. To maximize the deposited charge subject to the overpotential constraint, the weighting function $f(t)$ is unity, $A = \eta_0 - (\eta_0 - \eta_1)x(0)$, and $B = \eta_0 - \eta_1$.

To give insight into the solution, the following result gives a sufficient condition for the current that exactly meets the constraint to be optimal.

Theorem 3. *Suppose the integral Eq.*

$$\int_0^T i(\tau)(g_\eta(t-\tau) + Bg_x(t-\tau))d\tau = Af(t), \tag{19}$$

$t \in [0, T]$ has a solution $i(t)$. If $i(t) \ge 0$ then $i(t)$ is the solution to (18).

Proof. See Appendix □

Because (19) is a convolution, the solution can be easily found using Laplace Transforms.

$$i(t) = \mathcal{L}^{-1}\left\{ \left(G_\eta(s) + BG_x(s)\right)^{-1} \mathcal{L}\{Af(t)\} \right\}, \tag{20}$$

where the portion of $i(t)$ of interest is $t \in [0, T]$. In cases where $G_\eta(s) + BG_x(s)$ is strictly proper, for numerical solutions it is useful to utilize a non-constant function $f(t)$ where $f(0) = 0$, and $f(t)$ approaches unity quickly but sufficiently smoothly so that $i(t)$ is bounded.

3.2. Illustrative constraint charging analysis

As in the optimal charging analysis, it is insightful to analyze a battery model to interpret the theoretic results. To analyze the relevant internal variables, a thermodynamically consistent anode half-cell single-particle model was utilized that captures a multistep anode/electrolyte reaction mechanism and non-linear intercalation thermodynamics. The anode single-particle model, implemented in MATLAB, utilizes chemical kinetics and non-linear graphite intercalation activities presented in [30]. For the purposes of this study, the electrolyte is assumed to have constant potential and composition. The model dynamically resolves the anode bulk and surface lithium composition. The model is non-linear because it incorporates both chemical kinetics and non-ideal graphite intercalation activities. However, for relatively small perturbations, the non-linear model can have linear behaviors.

In this section, the implications of Theorem 3 are examined using this physically based model. In this case, the overpotential and intercalation fraction impulse response are obtained from the model. Once these responses are extracted, (20) is used to predict the optimal charging current.

A current pulse is imposed on the anode half-cell model and the surface intercalation fraction and overpotential response is obtained. Fig. 10 shows the impulse response of the overpotential, $g_\eta(t)$, and the intercalation fraction, $g_x(t)$ for the half-cell anode model at 25% and 75% SOC. Fig. 11 illustrates the optimal charging

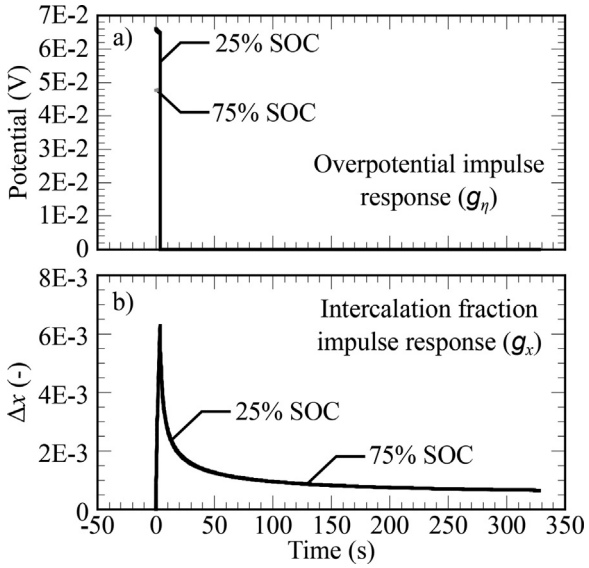

Fig. 10. Impulse response of Li-ion anode half-cell model at 75% SOC as defined in Colclasure et al. [30]. (a) Illustrates the overpotential response while (b) illustrates the intercalation fraction response at the anode surface from an imposed current density demand at the anode/electrolyte surface.

current as predicted by (20) for the half-cell anode model at 25% and 75% SOC using the impulse response shown in Fig. 10 with $f(t) = 1 - e^{-t}$. The optimal current has an initial impulse followed by a function decreasing to zero. Since $i(t)$ is always positive, it is optimal, and in this case, pulses or sinusoidal perturbations are not beneficial.

In actual implementation, the impulse would be replaced by a constant current until the constraint is active. The result is very similar to the constant current–constant voltage (CC–CV) protocol for battery charging, except in this case the current decreases to meet an internal constraint rather than keeping the external voltage constant.

Although this example was for a specific battery model, the type of analysis can be applied in general. In simulation or experimentation the optimal current trajectory can be determined by extracting the impulse responses ($g_\eta(t)$ and $g_x(t)$) and finding the solution to (20). If the solution to (20) is always positive, it is optimal, and exact to the optimization problem ((18)) is unnecessary.

4. Summary and conclusions

This paper utilizes basic system theoretic analysis of Li-ion battery systems to test the validity of physical, mechanistic explanations in minimizing losses and reducing lithium plating by

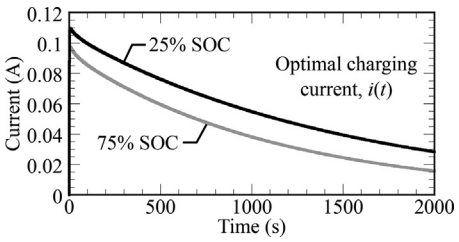

Fig. 11. Optimal charging current of the anode half-cell model at 25% and 75% SOC from (20). Since the optimal current is positive, it is also the optimal charging sequence for (18).

pulse charging. By assuming the battery dynamics (other than charge storage) are a linear and time-invariant, analytic solutions are obtained for both cases. In the case of minimized charging losses, the impedance spectra is related to optimal charging sequences. It is shown that for pulse charging to be optimal, the polar plot of the electrochemical impedance must approach the imaginary axis. Because the impedance of real batteries do not approach the imaginary axis, pulse charging is not optimal for reducing losses. In the analysis for charging while avoiding lithium plating, an overpotential constraint is imposed. Because this constraint is a function of intercalation fraction, both the intercalation fraction and overpotential impulse response are required to determine an optimal charging strategy. From these responses, the optimal current trajectory is derived. By using a physically based model, it is predicted that the optimal current strategy that reduces lithium plating is not sinusoidal. It should be emphasized that this paper does not provide definitive arguments for or against pulse charging or any evidence against any particular experimental results. However, this paper provides important guidance when considering a physical explanation for pulsed or sinusoidal charging benefits.

Acknowledgments

This research was supported by the Office of Naval Research via grant N00014-16-1-2780 and G. Tang was supported by NSF Grant CCF-1464205. We gratefully acknowledge frequent and insightful discussions with Prof. Robert J. Kee (Colorado School of Mines) on battery modeling generally. We are particularly grateful to Dr. Corey Love (Naval Research Laboratory) for sharing his experiences and measurements on pulsed-charging.

Appendix A. Definitions, lemmas, and preliminary results

A.1 Definitions, lemmas, and preliminary results

In this section, for complex number x, x^* is the complex conjugate of x.

Definition 2. Given function $x(t) \in L_2$ defined on the real line, the Fourier Transform of $x(t)$ is

$$X(j\omega) = \mathcal{F}\{x(t)\} \equiv \int_{-\infty}^{\infty} x(t) e^{-j\omega t} dt.$$

Definition 3. Given function $x(t) \in L_2[a, b]$,

$$\| x\|^2 = \int_a^b x^2(t) dt.$$

Lemma 4. (Plancharel's Theorem) [32]

Given functions $x(t)$, $y(t)$, $z(t) \in L_2 \cap L_1$ with Fourier Transforms $X(j\omega)$, $Y(j\omega)$, $Z(j\omega)$,

$$\int_{-\infty}^{\infty} x(t) y(t) dt = \frac{1}{2\pi} \int_{-\infty}^{\infty} X(j\omega)^* Y(j\omega) d\omega,$$

and

$$\int_{-\infty}^{\infty} \int_{-\infty}^{\infty} x(t) z(t-\tau) y(\tau) d\tau dt = \frac{1}{2\pi} \int_{-\infty}^{\infty} X(j\omega)^* Z(j\omega) Y(j\omega) d\omega. \quad (21)$$

Lemma 5. *Given $\hat{g}(t) \in L_2 \cap L_1$, $G(\hat{s}) = \mathcal{L}\{\hat{g}(t)\}$, with $\min_\omega \mathrm{Re}\{\hat{G}(j\omega)\} + \alpha \geq 0$. For $\eta \in L_2[0, T]$, the functional*

$$J(\eta) = \int_0^T \int_0^T \eta(t) \hat{g}(t-\tau) \eta(\tau) dt d\tau + \alpha \int_0^T \eta^2(t) dt,$$

satisfies

$$J(\eta) \geq \frac{\min_\omega \mathrm{Re}\{G(j\omega)\} + \alpha}{\pi} \| \eta\|^2.$$

Proof. Extend $\eta(t)$ to the infinite domain with zeros outside of $[0, T]$. Since η has finite support, $\eta \in L_1 \cap L_2$. Then using Lemma 4,

$$J(\eta) = \frac{1}{2\pi} \int_{-\infty}^{\infty} \eta(j\omega)^* (\hat{G}(j\omega) + \alpha) \eta(j\omega) d\omega,$$

where $\eta(j\omega)$ is the Fourier Transform of the extended $\eta(t)$. Thus

$$\begin{aligned} J(\eta) &= \frac{1}{2\pi} \int_{-\infty}^{\infty} (G(j\omega) + \alpha) |\eta(j\omega)|^2 d\omega \\ &= \frac{1}{\pi} \int_0^{\infty} (\mathrm{Re}\{G(j\omega)\} + \alpha) |\eta(j\omega)|^2 d\omega \\ &\geq \frac{1}{\pi} (\min_\omega \mathrm{Re}\{G(j\omega)\} + \alpha) \| \eta\|^2. \end{aligned}$$

□

Lemma 6. *Given $g(t), f(t) \in L_2 \cap L_1$, with $G(s) = \mathcal{L}\{g(t)\}$. If $\exists\ \varepsilon > 0$ such that $\frac{2\alpha}{\pi} \min_\omega (2\mathrm{Re}\{G(j\omega)\} + \alpha) > \varepsilon$, the solution $x(t)$ to the integral equation*

$$\int_0^T x(\tau)(g(t-\tau) + g(\tau - t)) d\tau + 2\alpha x(t) = f(t), \quad (22)$$

$t \in [0, T]$ satisfies

$$\int_0^T x^2(t) dt \leq \frac{1}{\varepsilon} \int_0^T f^2(t) dt. \quad (23)$$

Proof. Let $k(t) = g(t) + g(-t)$. Note that $k(t) = \mathcal{F}^{-1}\{K(j\omega)\}$ where $K(s) = G(s) + G(-s)$. Thus $K(j\omega) = G(j\omega) + G(-j\omega) = 2\mathrm{Re}\{G(j\omega)\}$ since $G(-j\omega) = G(j\omega)^*$. In addition, $\frac{2\alpha}{\pi}(K(j\omega) + \alpha) > \varepsilon$. Rewrite (22) as

$$f(t) = \int_0^T x(\tau) k(t-\tau) d\tau + 2\alpha x(t).$$

Via direct calculation,

$$\begin{aligned} \| f\|^2 = &\int_0^T \left(\int_0^T x(\tau) k(t-\tau) d\tau \right)^2 dt \\ &+ 4\alpha \int_0^T \int_0^T x(t) x(\tau) k(t-\tau) d\tau dt \\ &+ 4\alpha^2 \int_0^T x^2(t) dt. \end{aligned}$$

Extend $x(t)$ to the real line using zeros outside of $[0, T]$. Then

$$\begin{aligned} \| f\|^2 = &\int_0^T \left(\int_0^T x(\tau) k(t-\tau) d\tau \right)^2 dt \\ &+ 4\alpha \int_{-\infty}^{\infty} \int_{-\infty}^{\infty} x(t) x(\tau) k(t-\tau) d\tau dt \quad + 4\alpha^2 \int_{-\infty}^{\infty} x^2(t) dt. \end{aligned}$$

Note that the first term is always positive. Applying Lemma 4 to the second and third terms,

$$\begin{aligned}\|f\|^2 &\geq \frac{2\alpha}{\pi}\int_{-\infty}^{\infty}|X(j\omega)|^2K(j\omega)d\omega \\ &\quad+\frac{2\alpha^2}{\pi}\int_{-\infty}^{\infty}|X(j\omega)|^2d\omega \\ &=\frac{2\alpha}{\pi}\int_{-\infty}^{\infty}|X(j\omega)|^2(K(j\omega)+\alpha)d\omega \\ &\geq \frac{2\alpha}{\pi}\min_{\omega}(K(j\omega)+\alpha)\,\|x\|^2.\end{aligned}$$

□

A.2 Proof of Theorem 1

Under the assumptions of the theorem, the impulse response may itself contain an impulse function, i.e.

$$g(t)=\hat{g}(t)+\alpha\delta(t),$$

where $\hat{g}(t)$ is a bounded function, $\delta(t)$ is the dirac delta function, and $\alpha=\lim_{\omega\to\infty}G(j\omega)$. To avoid working with generalized functions, an equivalent to (2) is

$$v(t)=\int_0^T\hat{g}(t-\tau)i(\tau)d\tau+\alpha i(t)+v_{oc}(s_c(t)). \tag{24}$$

Let $\hat{G}(s)=\mathcal{L}\{\hat{g}(t)\}$. Since $G(j\omega)$ is strictly positive real, $\mathrm{Re}\{\hat{G}(j\omega)\}+\alpha>0$. Now,

$$\begin{aligned}\int_0^T i(t)v(t)dt &= \int_0^T i(t)\int_0^T\hat{g}(t-\tau)i(\tau)dtd\tau+\alpha\int_0^T i^2(t)dt \\ &\quad+\int_0^T v_{oc}(s_c(t))i(t)dt.\end{aligned}$$

Given (3), we have

$$\begin{aligned}\int_0^T v_{oc}(s_c(t))i(t)dt &= Q_0\int_0^T v_{oc}(s_c(t))\dot{s}_c(t)dt \\ &= Q_0\int_{s_c(0)}^{s_c(T)}v_{oc}(\psi)d\psi \\ &= v_{oc}(s_c(T))-v_{oc}(s_c(0)),\end{aligned}$$

so that this term depends only on the initial and final state of charge, and not the trajectory taken to arrive there. Since the initial state of charge is fixed and final state of charge is determined by the constraint $\int_0^T i(t)dt=Q$, this term is invariant over feasible trajectories, and the equivalent problem

$$\min_{i(t)\in L_2[0,T]}\int_0^T\int_0^T i(t)\hat{g}(t-\tau)i(\tau)dt\,d\tau+\alpha\int_0^T i^2(t)dt,$$

$$\text{subject to}\int_0^T i(t)dt=Q, \tag{25}$$

will have the same minimizer as (4).

Define the Lagrangian for this equivalent problem,

$$\begin{aligned}L(i,\mu)= &\int_0^T\int_0^T i(t)\hat{g}(t-\tau)i(\tau)dtd\tau+\alpha\int_0^T i^2(t)dt \\ &+\mu\left(\int_0^T i(t)dt-Q\right),\end{aligned}$$

where μ is a constant. Note that for feasible $i(t)$, the value of the Lagrangian is the same as the value of the objective function, so if $i(t)$ minimizes $L(i,\mu)$ for any fixed μ, $L(i,\mu)$ is a lower bound for the optimum of (25), while if $i(t)$ is also feasible (i.e. integrates to Q), it is a minimizer of (25).

Let $i^0(t)=(Q/\beta)\xi(t)$, as defined in the statement of Theorem 1, and consider $i(t)=i^0(t)+\eta(t)$ where $\eta(t)$ is an arbitrary function in $L_2[0,T]$. Via direct calculation,

$$L(i^0+\eta,\mu)=L(i^0,\mu)+\delta L(\eta,i^0,\mu)+\delta^2L(\eta),$$

where

$$\begin{aligned}\delta L(\eta,i^0,\mu) &= \int_0^T\left(\int_0^T i^0(\tau)k(t-\tau)d\tau+2\alpha i^0(t)+\mu\right)\eta(t)dt, \\ k(t-\tau) &= \hat{g}(t-\tau)+\hat{g}(\tau-t),\end{aligned}$$

and

$$\delta^2L(\eta)=\int_0^T\int_0^T\eta(t)\hat{g}(t-\tau)\eta(\tau)dtd\tau+\alpha\int_0^T\eta^2(t)dt.$$

Since $\xi(t)$ satisfies (5),

$$\int_0^T i^0(\tau)k(t-\tau)d\tau+2\alpha i^0(t)=\frac{Q}{\beta}$$

and $\delta L(\eta,\ i^0,\ -Q/\beta)=0$. By Lemma 5, $\delta^2L(\eta)\geq\frac{\mathrm{Re}\{G(j\omega)\}+\alpha}{\pi}\|\eta\|^2$. Thus, $L(i^0,-Q/\beta)\leq L(i^0+\eta,-Q/\beta)$ for all η and $i^0(t)$ is a minimizer of $L(i,-Q/\beta)$. Since $i^0(t)$ is also feasible, it is a minimizer of (25).□

A.3 Proof of Theorem 2

Let $h(t)$ be the solution to (6), and let $k(t)=g(t)+g(-t)$. Then the following are true

$$\begin{aligned}\int_0^\infty h(t)k(t-\tau)dt &= 1 \quad \tau\in[0,\infty), \\ \int_{-\infty}^T h(T-t)k(t-\tau)dt &= 1 \quad \tau\in(-\infty,T),\end{aligned}$$

where the second line follows from the first by redefining $t\to T-t$ and $\tau\to T-\tau$, while also using the fact that $k(t)$ is symmetric. By splitting the range of these integrals at $T/2$, rearranging, and adding and subtracting a term on each side, one obtains

$$\begin{aligned}&\int_0^{\frac{T}{2}}h(t)k(t-\tau)dt+\int_{\frac{T}{2}}^T h(T-t)k(t-\tau)dt= \\ &\quad 1-\int_{\frac{T}{2}}^\infty h(t)k(t-\tau)dt+\int_{\frac{T}{2}}^T h(T-t)k(t-\tau)dt,\end{aligned} \tag{26}$$

for $\tau\in[0,\infty)$, and

$$\begin{aligned}&\int_0^{\frac{T}{2}}h(t)k(t-\tau)d\,t+\int_{\frac{T}{2}}^T h(T-t)k(t-\tau)dt= \\ &\quad 1-\int_{-\infty}^{\frac{T}{2}}h(T-t)k(t-\tau)dt+\int_0^{\frac{T}{2}}h(t)k(t-\tau)dt,\end{aligned} \tag{27}$$

for $\tau\in(-\infty,T]$. Let $\zeta(t)$ be as defined in the theorem statement. Then

$$\begin{aligned}\int_0^T\zeta(t)k(t-\tau)dt &= \int_0^{\frac{T}{2}}h(t)k(t-\tau)dt \\ &\quad+\int_{\frac{T}{2}}^T h(T-t)k(t-\tau)dt.\end{aligned} \tag{28}$$

Using, (26) and (27),

$$\int_0^T\zeta(t)k(t-\tau)dt=1+z(\tau),$$

where

$$z(\tau)=\begin{cases}-\int_{\frac{T}{2}}^{\infty}h(t)k(t-\tau)dt & \\ \quad+\int_{\frac{T}{2}}^{T}h(T-t)k(t-\tau)dt & 0\le\tau\le\frac{T}{2}\\ -\int_{-\infty}^{\frac{T}{2}}h(T-t)k(t-\tau)dt & \\ \quad+\int_{0}^{\frac{T}{2}}h(t)k(t-\tau)dt & \frac{T}{2}<\tau\le T\end{cases}\tag{29}$$

Since $\int_0^T \xi(t)k(t-\tau)dt=1$ for $\tau\in[0,\,T]$,

$$\int_0^T(\zeta(t)-\xi(t))k(t-\tau)dt=z(\tau),$$

for $\tau\in[0,\,T]$. Note that $\mathrm{Re}\{G(j\omega)\}\ge\lim_{\omega\to\infty}G(j\omega)$ implies the conditions of Lemma 6 are met, so that

$$\int_0^T w_T^2(t)dt\le\frac{1}{\varepsilon}\int_0^T z^2(\tau)d\tau.$$

It remains to find an expression for $\int_0^T z(\tau)^2d\tau$. These expressions use the fact that because $g(t)$ represents a stable system and has a rational Laplace Transform, there exists K and $\beta>0$ such that $|g(t)|\le Ke^{-\beta t}$ for $t\ge0$. Bounds on $z(\tau)$ are calculated:

- $0\le\tau\le T/2$: Using (29), in this region, we have

$$\begin{aligned}z^2(\tau)&=\left(\int_{\frac{T}{2}}^{\infty}h(t)k(t-\tau)dt+\int_{\frac{T}{2}}^{T}h(T-t)k(t-\tau)dt\right)^2\\&\le\left(\int_{\frac{T}{2}}^{\infty}(|h(t)|+|h(T-t)|)Ke^{-\beta|t-\tau|}dt\right)^2\\&\le4\max_t|h(t)|^2\frac{K^2}{\beta^2}e^{-2\beta(T/2-\tau)}.\end{aligned}\tag{30}$$

- $T/2\le\tau\le T$: Due to symmetry, a similar argument as above gives

$$z^2(\tau)\le4\max_t|h(t)|^2\frac{K^2}{\beta^2}e^{-2\beta(\tau-T/2)}.\tag{31}$$

Bounds on $z(\tau)$ are then further developed over the following regions:

- $0\le\tau\le T/2-\ln(T)/\beta$: Using the fact that $\tau<T/2-\ln(T)/\beta$,

$$\begin{aligned}z^2(\tau)&\le4\max_t|h(t)|^2\frac{K^2}{\beta^2}e^{-2\ln(T)}\\&=4\max_t|h(t)|^2\frac{K^2}{T^2\beta^2}.\end{aligned}$$

- $0\le\tau\le T/2-\ln(T)/\beta$: A similar argument gives the same bound as above.
- $T/2-\ln(T)/(\beta)\le\tau\le T/2+\ln(T)/(\beta)$: Using (30) or (31) where the exponential term is less than 1,

$$z^2(\tau)\le4\max_t|h(t)|^2\frac{K^2}{\beta^2}.$$

Thus, multiplying each bound by the interval (overestimating the first and last interval as length $T/2$) and adding common terms,

$$\int_{-\infty}^{\infty}z(\tau)^2d\tau\le4\max_t|h(t)|^2\frac{K^2}{T\beta^2}+2\ln(T)4\max_t|h(t)|^2\frac{K^2}{\beta^2},$$

and $\frac{1}{T}\int_0^T w_T(\tau)^2d\tau\to0$ as $T\to\infty$.□

A.4 Proof of Theorem 3

Define inner product

$$\langle x,y\rangle=\int_0^T x(t)y(t)dt,$$

and let F be the linear mapping $F:L_2[0,\,T]\to L_2[0,\,T]$ given by

$$F(i)=\int_0^T i(\tau)k(t-\tau)d\tau,$$

where $k(t)=g_\eta(t)+Bg_x(t)$. Since $k(t)=0$ for $t<0$, $F(i)=\eta(t)+B\,x(t)$ where $\eta(t)$, and $x(t)$ are given by (16) and (17) respectively. Let f be the weighting function $f(t)$, and f_r the reverse time function $f(T-t)$. Then the optimization problem can be written as

$$\begin{aligned}\max_{i\in L_2[0,T]}\quad&\left\langle f_r,\mathrm{i}\right\rangle,\\\text{such that}\quad&F(i)\le Af.\end{aligned}$$

This is a linear optimization problem with dual [33]

$$\begin{aligned}\min_{\lambda\in L_2[0,T]}\quad&\left\langle\lambda,\mathrm{Af}\right\rangle,\\\text{such that}\quad&F^*(\lambda)=f_r,\\&\lambda\ge0,\end{aligned}$$

where F^* is the pullback of F, (i.e. $F^*(\lambda)=f_r$ indicates λ should satisfy $\langle\lambda,F(\cdot)\rangle=\langle f_r,\cdot\rangle$). When the dual problem has a feasible solution, it provides a upper bound on the primal problem. Let $i(t)$ be the solution to (19), and set $\lambda(t)=\frac{1}{A}i(T-t)$. Since $i(t)\ge0$, $\lambda(t)\ge0$. In addition, for arbitrary $x\in L_2[0,\,T]$

$$\begin{aligned}\langle\lambda,F(x)\rangle&=\int_0^T\lambda(t)\int_0^T x(\tau)k(t-\tau)d\tau dt\\&=\int_0^T\frac{1}{A}i(T-t)\int_0^T x(\tau)k(t-\tau)d\tau dt\\&=\int_0^T\int_0^T\frac{1}{A}i(T-t)k(t-\tau)x(\tau)dt\,d\tau\\&=\int_0^T\int_0^T\frac{1}{A}i(s)k(T-\tau-s)x(\tau)ds d\tau\\&=\int_0^T f(T-\tau)x(\tau)d\tau=\langle f_r,x\rangle.\end{aligned}$$

Thus, λ is feasible for the dual problem, and $\langle\lambda,\,Af\rangle$ is an upper bound on the optimal solution. In particular,

$$\langle\lambda,Af\rangle=\int_0^T i(T-t)f(t)dt.$$

On the other hand, $i(t)$ is feasible for the primal problem, with cost

$$\langle f_r,i\rangle=\int_0^T f(T-t)i(t)dt.$$

Since this is equal to the upper bound (by time reversal of the integration variable), $i(t)$ is optimal. □

References

[1] J. Newman, K.E. Thomas-Alyea, Electrochemical Systems, Wiley, Hoboken, NJ, 2004.
[2] G.L. Plett, Extended Kalman filtering for battery management systems of LiPB-based HEV battery packs, Part 3. State and parameter estimation, J. Power Sources 134 (2004) 277–292.
[3] J. Zhang, J. Lee, A review on prognostics and health monitoring of Li-ion battery, J. Power Sources 196 (2011) 6007–6014.
[4] B.K. Purushothaman, U. Landau, Rapid charging of lithium-ion batteries using pulsed currents: a theoretical analysis, J. Electrochem. Soc. 153 (2006) A533–A542.

[5] L.-R. Chen, Design of duty-varied voltage pulse charger for improving Li-ion battery-charging response, IEEE Trans. Ind. Electron. 56 (2009) 480–487.
[6] L.-R. Chen, S.-L. Wu, D.-T. Shieh, T.-R. Chen, Sinusoidal-ripple-current charging strategy and optimal charging frequency study for Li-ion batteries, IEEE Trans. Ind. Electron. 60 (2013) 88–97.
[7] L.-R. Chen, J.-J. Chen, C.M. Ho, S.-L. Wu, D.-T. Shieh, Improvement of Li-ion battery discharging performance by pulse and sinusoidal current strategies, IEEE Trans. Ind. Electron. 60 (2013) 5620–5628.
[8] J. Jiang, Q. Liu, C. Zhang, W. Zhang, Evaluation of acceptable charging current of power Li-ion batteries based on polarization characteristics, IEEE Trans. Ind. Electron. 61 (2014) 6844–6851.
[9] Y.-D. Lee, S.-Y. Park, Electrochemical state-based sinusoidal ripple current charging control, IEEE Trans. Power Electron. 30 (2015) 4232–4243.
[10] F. Savoye, P. Venet, M. Millet, J. Groot, Impact of periodic current pulses on Li-ion battery performance, IEEE Trans. Ind. Electron. 59 (2012) 3481–3488.
[11] P. Keil, A. Jossen, Charging protocols for lithium-ion batteries and their impact on cycle life – an experimental study with different 18650 high-power cells, J. Energy Storage 6 (2016) 125–141.
[12] S.-Y. Cho, I.-O. Lee, J.-I. Baek, G.-W. Moon, Battery impedance analysis considering DC component in sinusoidal ripple-current charging, IEEE Trans. Ind. Electron. 63 (2016) 1561–1573.
[13] S.S. Zhang, K. Xu, T.R. Jow, Study of the charging process of a $LiCoO_2$-based Li-ion battery, J. Power Sources 160 (2006) 1349–1354.
[14] R. Methekar, V. Ramadesigan, R.D. Braatz, V.R. Subramanian, Optimum charging profile for lithium-ion batteries to maximize energy storage and utilization, ECS Trans. 25 (2010) 139–146.
[15] R. Klein, N.A. Chaturvedi, J. Christensen, J. Ahmed, R. Findeisen, A. Kojic, Optimal charging strategies in lithium-ion battery, American Control Conference (ACC), (2011) , pp. 382–387.
[16] H.E. Perez, X. Hu, S.J. Moura, Optimal charging of batteries via a single particle model with electrolyte and thermal dynamics, American Control Conference (ACC), (2016) , pp. 4000–4005.
[17] J. Liu, G. Li, H.K. Fathy, A computationally efficient approach for optimizing lithium-ion battery charging, J. Dyn. Syst. Meas. Control 138 (2) (2016) 021009.
[18] S. Pramanik, S. Anwar, Electrochemical model based charge optimization for lithium-ion batteries, J. Power Sources 313 (2016) 164–177.
[19] A. Abdollahi, X. Han, G.V. Avvari, N. Raghunathan, B. Balasingam, K.R. Pattipati, Y. Bar-Shalom, Optimal battery charging. Part I: minimizing time-to-charge, energy loss, and temperature rise for OCV-resistance battery model, J. Power Sources 303 (2016) 388–398.
[20] H. Perez, X. Hu, S. Dey, S. Moura, Optimal charging of Li-ion batteries with coupled electro-thermal-aging dynamics, IEEE Trans. Veh. Technol. (2017).
[21] E. Namor, F. Sossan, D. Torregrossa, R. Cherkaoui, M. Paolone, Battery storage system optimal exploitation through physics-based model predictive control, Powertech, number EPFL-CONF-228847, (2017) .
[22] A.V. Oppenheim, A.S. Willsky, Signals and Systems, 2nd ed., Pearson, 2014.
[23] H.L. Van Trees, Detection, Estimation, and Modulation Theory, Wiley, 1968.
[24] W.R. Derrick, Complex Analysis and Applications, 2nd ed., Wadsworth, 1984.
[25] S. Mohan, Y. Kim, A.G. Stefanopoulou, Energy-conscious warm-up of Li-ion cells from subzero temperatures, IEEE Trans. Ind. Electron. 63 (2016) 2954–2964.
[26] S. Mohan, J. Siegel, A.G. Stefanopoulou, M. Castanier, Y. Ding, Synthesis of an energy-optimal self-heating strategy for Li-ion batteries, IEEE Conf. Decision and Control (CDC), (2016) , pp. 1589–1594.
[27] S. Mohany, Y. Kim, A.G. Stefanopoulou, Y. Ding, On the warmup of Li-ion cells from sub-zero temperatures, American Control Conference (ACC), (2014) , pp. 1547–1552.
[28] M. Farkhondeh, M. Pritzker, M. Fowler, M. Safari, C. Delacourt, Mesoscopic modeling of Li insertion in phase-separating electrode materials: application to lithium iron phosphate, Phys. Chem. Chem. Phys. 16 (41) (2014) 22555–22565.
[29] M. Guo, G. Sikha, R.E. White, Single-particle model for lithium-ion cell: thermal behavior, J. Electrochem. Soc. 158 (2011) A122–A132.
[30] A.M. Colclasure, R.J. Kee, Thermodynamically consistent modeling of elementary electrochemistry in lithium-ion batteries, Electrochim. Acta 55 (2010) 8960–8973.
[31] C. Uhlmann, J. Illig, M. Ender, R. Schuster, E. Ivers-Tiffée, In situ detection of lithium metal plating on graphite in experimental cells, J. Power Sources 279 (2015) 428–438.
[32] K. Yosida, Functional analysis, Classics in Mathematics, Springer, Berlin, Heidelberg, 1995.
[33] S. Boyd, L. Vandenberghe, Convex Optimization, Cambridge University Press, 2004.